Pamukkale Univ Muh Bilim Derg, 32(5), 948-961, 2026

Pamukkale Üniversitesi Mühendislik Bilimleri Dergisi

Pamukkale University Journal of Engineering Sciences

Investigating DC microgrids based on centralized protection: A case study of BTS

Merkezi korumaya dayalı DC mikro şebekelerin incelenmesi: Bir BTS durum çalışması

Mohammad Reza Kochehbiuki[1*], *Alireza Sedighi Anaraki*[1], *Mohammad Reza Mazidi*[1]

[1]Department of Electrical Engineering, Faculty of Engineering, Yazd University, Yazd, Iran.
1269mrk1269@gmail.com, sedighi@yazd.ac.ir, mrmazidi@yazd.ac.ir

Received/Geliş Tarihi: 06.10.2025 Revision/Düzeltme Tarihi: 09.12.2025 doi: 10.65206/pajes.45725
Accepted/Kabul Tarihi: 29.12.2025 Research Article/Araştırma Makalesi

Abstract

This research presents an innovative protection strategy tailored for centralized DC microgrids specifically designed for base transceiver stations (BTS). The method leverages the similarity in the rate of current change measured simultaneously at both ends of a line segment to detect internal faults effectively. The approach addresses key challenges in microgrid protection including the detection of high-resistance faults, distinguishing between permanent and transient fault conditions, and safeguarding critical components such as loads, photovoltaic arrays, and batteries. It also considers the resilience of the system in the event of failures in line sensors and circuit breakers. Unlike conventional protection schemes that depend heavily on both voltage and current measurements, the proposed system offers a cost-efficient alternative. It operates with a single centralized intelligent electronic device (IED) overseeing the entire microgrid, complemented by only one current sensor installed at each end of every line segment. This streamlined configuration simplifies hardware requirements without compromising detection accuracy. The reliability and effectiveness of the protection mechanism have been rigorously validated through comprehensive simulations conducted in MATLAB/Simulink. The tests encompassed both internal faults within the microgrid and external fault scenarios, demonstrating robust performance under various operational conditions. This work contributes to advancing protection schemes for DC microgrids, which are increasingly pivotal for sustainable and efficient energy management in telecommunication infrastructure. It aligns with contemporary trends and challenges in microgrid protection, emphasizing economical design and dependable fault management.

Keywords: Central protection, Cosine similarity index (CSI), DC microgrid, High resistance, BTS.

Öz

Bu araştırma, özellikle baz istasyonu verici/alıcıları (BTS) için tasarlanmış merkezi DC mikro şebekelere yönelik yenilikçi bir koruma stratejisi sunmaktadır. Yöntem, bir hat kesitinin her iki ucunda aynı anda ölçülen akım değişim oranındaki benzerlikten yararlanarak dahili arızaların etkin bir şekilde tespit edilmesini sağlamaktadır. Yaklaşım, mikro şebeke korumasındaki temel zorluklara çözüm getirmektedir; bunlar arasında yüksek dirençli arızaların tespiti, kalıcı ve geçici arıza durumlarının ayırt edilmesi, yükler, fotovoltaik diziler ve bataryalar gibi kritik bileşenlerin korunması yer almaktadır. Ayrıca hat sensörleri ve devre kesicilerde meydana gelebilecek arızalar karşısında sistemin dayanıklılığını da dikkate almaktadır. Geleneksel koruma yöntemlerinin hem gerilim hem de akım ölçümlerine yoğun biçimde bağımlı olmasının aksine, önerilen sistem maliyet açısından verimli bir alternatif sunmaktadır. Tüm mikro şebekeyi denetleyen tek bir merkezi akıllı elektronik cihaz (IED) ile çalışmakta, her hat kesitinin yalnızca iki ucuna birer akım sensörü yerleştirilmesi yeterli olmaktadır. Bu sadeleştirilmiş yapı, donanım gereksinimlerini basitleştirirken tespit doğruluğundan ödün vermemektedir. Koruma mekanizmasının güvenilirliği ve etkinliği MATLAB/Simulink ortamında gerçekleştirilen kapsamlı benzetimlerle titizlikle doğrulanmıştır. Testler hem mikro şebeke içindeki dahili arızaları hem de harici arıza senaryolarını kapsayarak çeşitli işletme koşullarında güçlü bir performans ortaya koymuştur. Bu çalışma, telekomünikasyon altyapısında sürdürülebilir ve verimli enerji yönetimi için giderek daha kritik hale gelen DC mikro şebekeler için koruma şemalarının geliştirilmesine katkıda bulunmaktadır. Çalışma, mikro şebeke korumasındaki güncel eğilimler ve zorluklarla uyumlu olup ekonomik tasarım ve güvenilir arıza yönetimini vurgulamaktadır.

Anahtar kelimeler: Merkezi koruma, Kosinüs benzerlik endeksi, DC mikro şebeke, Yüksek direnç, BTS.

1 Introduction

Microgrid technology has rapidly evolved as a crucial solution for ensuring uninterrupted and sustainable power supply, particularly for remote and critical infrastructures like telecommunication base transceiver stations (BTS). BTS, which increasingly rely on hybrid DC microgrids for sustainable operation, present unique protection challenges that existing AC-derived solutions fail to address adequately [1]-[3].

DC microgrids have garnered attention due to several inherent advantages over their AC counterparts. Their compatibility with DC-based renewable resources such as photovoltaic arrays and batteries eliminates the need for multiple power conversions, thereby improving system efficiency and simplifying control [4]-[6]. This makes DC microgrids especially suitable for telecom applications, where power quality and reliability are paramount [7],[8].

However, protection of DC microgrids is more challenging than traditional AC systems. Unlike AC systems, DC lacks a natural current zero crossing, which complicates fault detection and clearance. Consequently, rapid and accurate fault diagnosis is essential to prevent damage to sensitive equipment and minimize service interruptions [9],[10]. Protection limitations in non-unitary methods (overcurrent, impedance-based) lack selectivity during load fluctuations [11]-[13] and in unitary methods (differential protection) fail for high-resistance faults

*Corresponding author/Yazışılan Yazar

($Rf \geq 0.8\ \Omega$) [14]-[16]. Existing protection approaches often require multiple sensors and rely on both voltage and current measurements, increasing system cost and complexity [11],[13].

There is a pressing need for a protection strategy that minimizes hardware while ensuring fast, selective, and reliable fault detection. Centralized protection schemes have shown promise in this regard, as they can leverage communication capabilities within the microgrid to optimize sensor use and fault analysis [12],[17].

This study introduces a centralized protection method for DC microgrids supporting BTS, which uses current sensors only at the ends of line segments. By employing cosine similarity to compare the rate of current change at both ends, the scheme effectively distinguishes internal faults from external disturbances. Furthermore, it differentiates permanent faults from transient ones, enabling timely reconnection after temporary faults and reducing unnecessary outages. The current of each DC microgrid line segment is transmitted to a central IED. Using data from adjacent line sections, the central IED overcomes the failure problem from each location and accurately generates the operating signal for the corresponding circuit breaker on the fault section. The performance results of the proposed method are simulated for different cases, including high resistance faults, in MATLAB/Simulink environments.

This approach aligns with telecom operators' needs for resilient, maintenance-friendly protection systems while accommodating future expansions like 5G power infrastructure and vehicle-to-grid integration [2],[8].

In continue in section 2 scientific foundation is explained. The network, challenges, and solutions are introduced in 3 simulations are shown in 4 And finally results are explained in 1.

2 Scientific foundations

Waveform similarity analysis employs several computational techniques to quantify signal correspondence. Among these, three principal methodologies are widely implemented: Pearson's product-moment correlation, Euclidean norm comparisons, and cosine similarity assessment [18]. The cosine-based approach demonstrates particular advantages for power system applications due to its amplitude invariance and superior fault detection precision [19]. This vector analysis technique evaluates waveform likeness through angular relationships rather than magnitude differences.

The mathematical basis originates from vector dot products. For two measurement vectors $\vec{x}$ and $\vec{y}$, their dot product is calculated as:

$$\vec{x} \cdot \vec{y} = \sum_{i=1}^{n} x_i y_i = x_1 y_1 + x_2 y_2 + \cdots + x_n y_n \tag{1}$$

This scalar operation enables subsequent similarity assessments. The geometric interpretation relates this product to vector magnitudes and their included angle:

$$\vec{x} \cdot \vec{y} = \|\vec{x}\| \times \|\vec{y}\|\, cos(\theta) = \|\vec{y}\| \times \|\vec{x}\|\, cos(\theta) \tag{2}$$

From this fundamental relationship, we derive the cosine of the angle between vectors:

$$cosine\ similarity\ (CS) = cos(\theta) = \frac{\vec{x} \cdot \vec{y}}{\|\vec{x}\| \times \|\vec{y}\|} \tag{3}$$

Equation (3) can be used to calculate the value of the cosine of the angle between two vectors, indicating the measurement of the direction instead of the value (magnitude).

In addition to the angle between two vectors, the cosine similarity relationship also shows the similarities between vectors (direction). Considering the two vectors X and Y, the cosine similarity between them is calculated from Equation (4).

$$CS = \frac{X \,.\, Y}{|X|\,|Y|} = \frac{\sum_{i=1}^{n}(X_i Y_i)}{\sqrt{\sum_{i=1}^{n}(X_i)^2}\sqrt{\sum_{i=1}^{n}(Y_i)^2}} \tag{4}$$

Basically, CS shows the relative orientation of the vectors and is independent of their magnitude. $CS \in [-1, 1]$, where $CS = 1$ indicates that both vectors are in the same direction and $CS = -1$ indicates that they are in the opposite directions. CS value for two orthogonal vectors is zero, indicating zero similarity [20]. These are shown in Figure 1.

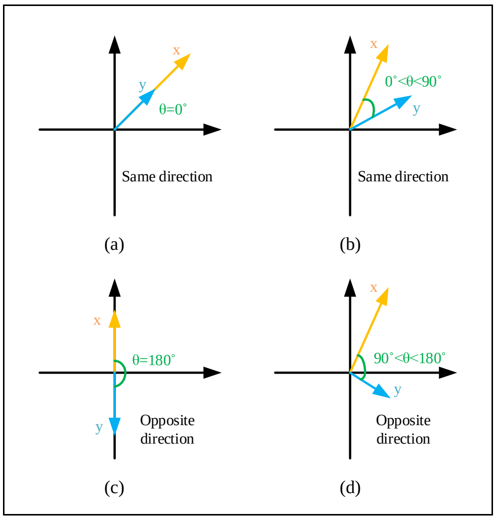

Figure 1. Direction diagrams for different vectors.
(a): Two vectors with the same direction ($\theta = 0^{\circ}$).
(b): Two vectors with the same direction ($0^{\circ} < \theta < 90^{\circ}$).
(c): Two vectors with opposite directions ($\theta = 180^{\circ}$), d) Two vectors with opposite directions ($90^{\circ} < \theta < 180^{\circ}$) [21].

Given the above explanation, the cosine similarity algorithm can effectively measure the similarity of two independent vectors. The cosine similarity describes the angle between two vectors, indicating the difference in direction rather than location and size [21]. Figure 2. shows the flowchart of the cosine similarity algorithm.

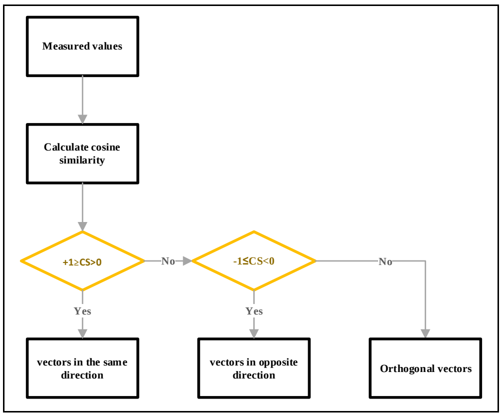

Figure 2. Performance of cosine similarity algorithm.

3 The network, challenges, and solutions

The study focuses on a 48V DC microgrid system with 3.5 kW capacity designed for BTS applications. As shown in Figure 3, the system architecture integrates multiple critical components including photovoltaic generation through DC-DC boost converters, energy storage via bidirectional DC-DC converters, grid interconnection using voltage source converters (VSC), and dedicated loads for 3G (0.48 kW) and 4G (3.024 kW) telecommunications equipment.

During standard operation, the microgrid preferentially utilizes local PV generation, resorting to main grid power only during production deficits. The system operates in two distinct modes: islanded mode where battery converters maintain voltage stability by balancing production and demand, and grid-connected mode where the VSC regulates voltage at the point of common coupling (PCC).

The protection system builds upon the framework established in [10], implementing zone-based protection with solid-state circuit breakers (SSCBs) defining each section. A centralized intelligent electronic device (IED) provides comprehensive system monitoring, supported by dual-ended current measurement for precise fault detection and localization. This configuration introduces several key enhancements to the baseline architecture.

Critical innovations include advanced fault persistence analysis using auto reclosing with waveform reevaluation to distinguish transient (under 2ms) from permanent faults, along with component-specific protection mechanisms for PV arrays, battery banks, and telecom loads. The system provides complete fault coverage for both line-to-line (L-L) and line-to-ground (L-G) faults across all impedance conditions, from low-impedance ($Rf < 0.8\,\Omega$) to high-impedance ($Rf \leq 0.8\,\Omega$) scenarios.

Protection logic employs a hierarchical decision-making process beginning with initial fault detection through disturbance index thresholding, followed by fault zone identification via current waveform correlation. The system then verifies fault persistence before initiating breaker operation and activates specialized component protection when faults occur outside line segments. This comprehensive approach effectively addresses the transient fault handling and distributed energy resource (DER) protection limitations noted in [10], while maintaining full compatibility with existing microgrid control systems.

3.1 Low impedance faults

DC microgrids demonstrate unique fault behaviors under low-impedance conditions due to their minimal line resistance. When faults occur, the rapid discharge of converter capacitive elements generates extremely steep current surges ($di/dt > 5000\,A/ms$) within sub-millisecond timeframes [9],[22]. These severe transients can drive system voltages beyond operational limits, exceed the rated capacity of semiconductor devices in power converters, and sustain dangerous arcing conditions that lack natural current zero-crossings. Fault currents typically reach magnitudes 8-10 times greater than nominal values, creating two significant protection challenges that must be addressed.

The first challenge involves detection sensitivity, where current derivatives provide rapid response times ($< 100\,\mu s$) but local measurements alone cannot determine fault location precisely, requiring supplemental communication for accurate zone identification [10]. The second challenge relates to arc interruption complexity, as sustained DC arcing damages contacts and necessitates forced current zero techniques along with ultra-fast solid-state breakers for effective protection.

Modern protection solutions address these challenges by combining several approaches. Local current derivative monitoring (Equation (3)) works in conjunction with centralized differential protection and directional current analysis to achieve both speed and selectivity in fault detection. This integrated hybrid approach maintains system security during 115% overload conditions while reliably detecting faults within 0.5ms [10], providing comprehensive protection against the unique challenges posed by low-impedance faults in DC microgrids.

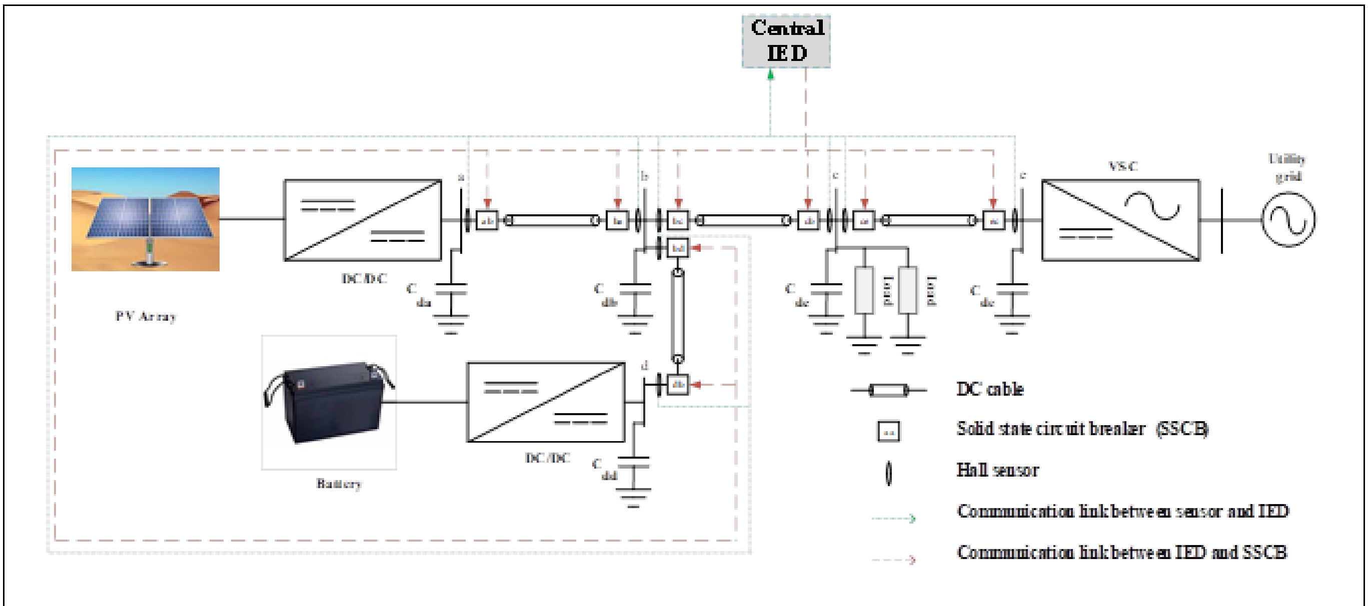

Figure 3. The simulated DC microgrid circuit related to BTS.

3.2 High impedance faults

High-impedance ground faults ($Rf \geq 0.8\,\Omega$) create distinctive diagnostic challenges for DC microgrid protection systems, particularly when occurring through indirect paths such as vegetation contact or human exposure. These faults generate relatively low currents below the system's 72.9A nominal rating (for the 3.5kW/48V test configuration), leading to several complex detection issues that conventional protection methods struggle to address effectively.

The primary challenge stems from signal ambiguity, where fault currents in the 10-50A range closely mimic normal system behavior including load variations from 3G/4G traffic spikes, scheduled equipment cycling, and fluctuations in renewable generation output. This similarity makes reliable fault identification particularly difficult. Conventional protection schemes face significant limitations in these scenarios, as differential current (I_{diff}) becomes undetectable below the $0.8\,\Omega$ threshold (Figure 4), directional relays cannot reliably identify phase angle shifts, and overcurrent elements fail to distinguish between actual faults and normal load variations in the 86-115% range.

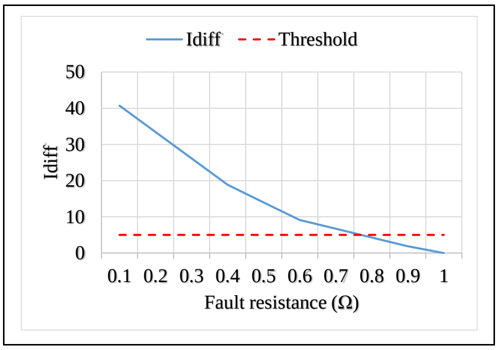

Figure 4. Current difference along a high resistance internal fault.

Further complicating detection is the waveform distortion characteristic of DC systems, where the absence of natural zero-crossings combines with non-linear arc behavior and intermittent fault contact to produce erratic current signatures that traditional protection algorithms cannot interpret reliably. These distorted waveforms often confuse conventional protection schemes, leading to either failure to operate or unnecessary tripping.

To overcome these challenges, the proposed protection strategy implements several advanced techniques. Dynamic adjustment of the Cosine Similarity Index (CSI) thresholds (Equation (4)) allows for sensitive detection across varying fault conditions. The system employs multi-variable waveform correlation analysis to distinguish genuine faults from normal system transients, supplemented by sequential fault verification logic to confirm fault persistence before initiating protective actions. This comprehensive approach maintains reliable operation while addressing the unique

difficulties posed by high-impedance faults in DC microgrid environments.

To address these protection challenges, we have developed a centralized system that analyzes current waveform correlations in DC microgrids, providing accurate discrimination between low-impedance faults ($Rf < 0.8\,\Omega$) and high-impedance faults ($Rf \geq 0.8\,\Omega$). The system is specifically designed for 48V DC microgrid configurations with a 3.5kW power capacity and 72.9A nominal current rating.

The protection scheme establishes a high-resistance fault threshold at $0.8\,\Omega$, which is carefully determined based on the system's electrical characteristics where 72.9 A corresponds to a $0.65\,\Omega$ equivalent resistance. This threshold setting incorporates a 23% safety margin above the theoretical $0.65\,\Omega$ value to ensure reliable operation. The classification methodology identifies any fault that reduces current below the 72.9A nominal rating ($Rf > 0.65\,\Omega$) as a high-resistance condition.

Central to the system's operation is its advanced current similarity analysis, which enables consistent fault detection across the full spectrum of possible fault impedances. This analytical approach examines waveform correlations to distinguish between different fault types while maintaining protection reliability during normal system operation. The $0.8\,\Omega$ threshold serves as a critical demarcation point in the protection logic, separating the detection and response strategies for low-impedance and high-impedance fault conditions.

4 Simulation

The simulated microgrid model (Figure 3) incorporates distinct protection zones, with current measurements transmitted from sensors on both ends of the line to the IED. Based on this data, the IED issues appropriate protection command to each zone. To analyze fault behavior (as illustrated in Figure 5), various fault scenarios are intentionally introduced within the network.

Building on the framework established in [10], this study examines fault detection and classification in the microgrid (Figure 3}) (Section 4.1), focusing on both internal and external faults through current value analysis (Section 4.2)and protection performance evaluation using the CSI (Section 4.3). A critical aspect of this work involves distinguishing transient faults from permanent faults, which is essential for ensuring reliable microgrid operation. Additionally, the protection strategies for key components-including loads, PV arrays, batteries, and other critical equipment are thoroughly analyzed to ensure robustness under fault conditions. Finally, the proposed algorithm for integrated fault management is presented, offering a comprehensive solution for microgrid protection.

4.1 High fault detection

The protection system employs a disturbance index (Di) to identify faults using current measurements from line sensors. The index is computed as:

$$Di = \frac{1}{N \times \Delta t} \times \left(\sum_{n=1}^{N} |i_{n+1} - i_n|\right) \quad (5)$$

The disturbance index (Di) is computed from current measurements obtained by the IED's sensors, where i_n represents the current value at the n^{th} sampling instant. With four samples acquired within a 1ms window (N=4) and Δt denoting the sampling interval, the index calculation considers only the absolute values of current differences to monitor magnitude variations. A fault is confirmed when Di exceeds the threshold ζ, which is derived from the predetermined condition that the sum of four consecutive current differences equals 5A. This threshold value is calculated as:

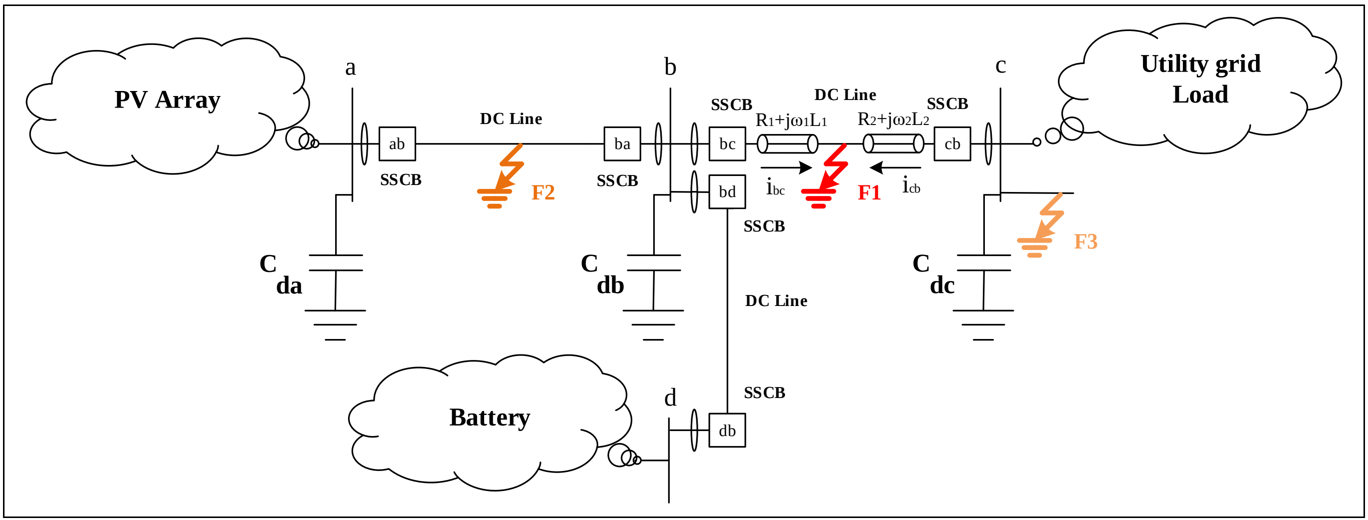

Figure 5. The simulated DC microgrid and the location of faults F_1 and F_2 of high impedance type and F_3 of low impedance type.

$$\zeta = \frac{1}{N\times\Delta t}\times(\sum_{n=1}^{N}|i_{n+1}-i_n|) = \frac{1\times 5}{4\times 250\times 10^{-6}} = 5000\,{}^{A}/_{s} \quad (6)$$

The selection of $\sum_{n=1}^{N}|i_{n+1}-i_n| = 5A$ ensures secure IED operation, with the system remaining in normal state when the measured disturbances stay below this threshold. The absolute value operation in Equation (5) serves to eliminate directional dependence, focusing solely on the magnitude of current changes for reliable fault detection.

It is worth noting that the disturbance index increases even for load change or any other switching phenomenon.

4.2 Current values during internal and external fault

The protection scheme examines current directional characteristics to discriminate between internal and external faults within the microgrid. For internal faults occurring at busbar b, the transient response of line current i_{bc} during fault condition F_1 can be modeled through the RLC network representation:

$$i_{bc}(s) = \frac{\frac{V_{db}(0)}{L_1}+i_{bc}(0)}{s^2+\frac{R_1}{L_1}s+\frac{1}{L_1C_{db}}} \quad (7)$$

where $V_{db}(0)$ is the voltage across the capacitor C_{db} in busbar b, and $i_{bc}(0)$is the current passing through L_1 of the DC line at the moment of the fault. The current fault component in the time domain can be expressed as follows:

$$i_{bc}^{F1}(t) = \frac{V_{db}(0)}{L_1(m_2-m_1)}(e^{-m_1t}-e^{-m_2t}) + \frac{i_{bc}(0)}{m_2-m_1}(m_2e^{-m_2t} - m_1e^{-m_1t}) \quad (8)$$

In Equation (8), its parameters are defined as follows:

$$m_1 = -a_1 + \sqrt{a_1^2-\omega_0^2}$$
$$m_2 = -a_1 - \sqrt{a_1^2-\omega_0^2} \quad (9)$$
$$a_1 = \frac{R_1}{2L_1}$$
$$\omega_1 = \sqrt{\frac{1}{L_1C_{db}} - (\frac{R_1}{2L_1})^2}$$
$$\omega_0 = \sqrt{a_1^2+\omega_1^2}$$

The time derivative of Equation (8) for $t = 0^+$ at the moment of the fault is as follows:

$$\frac{di_{bc}(t)}{dt} = \frac{V_{db}(0)}{L_1} - 2a_1 i_{bc}(0) \quad (10)$$

The relationship described in Equation (10) demonstrates that the magnitude of current variation is fundamentally dependent on two key factors: the initial voltage conditions across the DC capacitor and the pre-fault line current characteristics. Applying these principles to busbar c during an F_1 fault scenario, the resulting change in line current can be quantified as i_{cb}, as derived from the governing equations. This analysis highlights the critical influence of pre-fault operating conditions on fault current behavior in the system.

$$\frac{di_{cb}(t)}{dt} = \frac{V_{dc}(0)}{L_2} - \frac{R_2}{L_2} i_{cb}(0) \quad (11)$$

For internal fault F_1, the solutions to Equations (10) and (11) yield positive values when evaluated against the conventional current direction defined in Figure 5. In contrast, external fault F_2 presents a distinct signature where these same equations produce values of equal magnitude but opposite polarity, as illustrated in Figure 5. During an F_2 fault event, the current variations i_{bc} and i_{cb} exhibit specific behavioral patterns that can be characterized as follows:

$$\frac{d(-i_{bc}(t))}{dt} = \frac{-di_{bc}(t)}{dt}$$
$$\frac{-di_{bc}(t)}{dt} = -\frac{V_{db}(0)}{L_1} + \frac{R_1}{L_1} i_{bc}(0)$$
$$\frac{di_{cb}(t)}{dt} = \frac{V_{dc}(0)}{L_2} - \frac{R_2}{L_2} i_{cb}(0) \quad (12)$$
$$\frac{-di_{bc}(t)}{dt} = \frac{di_{cb}(t)}{dt}$$

4.3 Protection performance based on cosine similarity index (CSI)

The CSI is employed by the IED to perform protection functions. To compute the CSI, current samples are collected from both ends of the line over a 2 ms window, with measurements taken at 0.25ms intervals. These samples are used to analyze the currents i_{cb} and i_{cb} as follows:

$$x_i = \frac{di_{bc}(t)}{dt} = \frac{i_{bc}(t_{i+1}) - i_{bc}(t_i)}{t_{i+1} - t_i}$$
$$X = average\{x_1, x_2, \dots, x_7\} = average\left\{\frac{di_{bc1}}{dt}, \frac{di_{bc2}}{dt}, \dots \frac{di_{bc7}}{dt}\right\}$$
$$Y = average\{y_1, y_2, \dots, y_7\} = average\left\{\frac{di_{cb1}}{dt}, \frac{di_{cb2}}{dt}, \dots \frac{di_{cb7}}{dt}\right\} \quad (13)$$

Using Equation (13), the CSI can be calculated as follows:

$$CSI = \frac{X \cdot Y}{|X||Y|} = \frac{\frac{1}{7}\sum_{n=1}^{7} x_n \frac{1}{7}\sum_{n=1}^{7} y_n}{\left|\frac{1}{7}\sum_{n=1}^{7} x_n\right|\left|\frac{1}{7}\sum_{n=1}^{7} y_n\right|} = \frac{\sum_{n=1}^{7} x_n \cdot \sum_{n=1}^{7} y_n}{|\sum_{n=1}^{7} x_n||\sum_{n=1}^{7} y_n|} \quad (14)$$

Based on the analysis of internal and external faults, the CSI yields distinct values corresponding to different fault conditions:

$$CSI = \begin{cases} +1, if, internal\ fault; \\ -1, \quad if, external; \end{cases} \quad (15)$$

4.4 Protection of loads, PV array, and battery

When the protection system identifies an external fault condition ($CSI = -1$) across all line segments, it initiates specialized routines to locate faults within individual microgrid components. The detection methodology varies for different elements:

4.4.1 PV array protection

Faults in the PV subsystem are identified through directional current monitoring at the converter interface. The algorithm detects current reversals flowing toward the array instead of the DC bus.

4.4.2 Detecting faults in microgrid loads

In the proposed protection scheme, given the use of the central IED and with the help of adjacent sensors, the fault is detected. In this way, we investigate the current data sent from the sensors to the central IED, and if the received current increases many times, the operation command is sent to the adjacent load breakers. However, in some cases, this rise in current may be due to a sudden increase in load current, requiring measures to be taken to prevent the occurrence of incorrect operation. To solve this problem, for the protection of loads, such as fixed loads, there must be telecommunication posts at the entrance of each post of a circuit breaker, and a current threshold is required to be defined for the loads. Thus, a current threshold is determined in case of disconnection or the addition of such loads through circuit breakers for protection.

4.4.2.1 Current threshold determination for load protection

To reliably distinguish genuine fault conditions from normal load transients-such as sudden variations in BTS traffic-a well-defined current threshold I_{th} is required. This threshold is formulated using the rated load current I_{rated} and a safety margin coefficient k:

$$I_{th} = k \times I_{rated} \quad (16)$$

The coefficient k is selected to ensure that the protection system remains secure during normal operational fluctuations without compromising sensitivity to actual faults. In BTS telecommunication applications, load current naturally varies due to dynamic traffic patterns and equipment switching. These fluctuations typically span from approximately 85% to 115% of the nominal load current, reflecting conditions such as the temporary disconnection or reconnection of a 3G telecommunication post.

To prevent unnecessary or nuisance tripping, the threshold factor must be set above the maximum expected normal fluctuation. Accordingly, $k = 1.25$ is adopted, providing an adequate margin beyond the upper bound of the observed range (≈115%). This additional margin also accounts for sensor tolerances, measurement noise, manufacturing deviations, and minor unmodeled transient behaviors that may appear during normal operation.

The IED classifies an event as a fault only when the measured current exceeds I_{th} for a predefined minimum duration (e.g., several milliseconds). This criterion ensures selective and reliable operation while maintaining robustness against transient load variations inherent in BTS microgrid environments.

4.4.3 Battery protection

In the DC microgrid, the current direction in the battery is bidirectional. In case of a fault in the battery, the direction of the current changes towards the battery, which is the same as when the battery is being charged, causing a mistake in the protection function. To prevent malfunction, a current threshold is defined to protect the battery. When a fault occurs in the battery and after being detected, the central IED sends the necessary command to the circuit breaker of the battery line.

4.5 Distinguishing transient faults from the permanent ones

In the presented protection scheme, by distinguishing transient faults from permanent ones and separating them, an attempt is made to reduce network outages due to temporary faults. The detailed flowchart of the proposed protection scheme is presented in Figure 6. As shown in the flowchart, after distinguishing the fault in the microgrid and sending the command to the circuit breakers, the circuit breakers are reconnected, and the data received from the sensors is checked. If the fault is fixed, the microgrid works normally; otherwise, the function command is sent to the circuit breakers.

4.6 Comparative evaluation of the proposed CSI-Based protection scheme

To strengthen the technical justification for the proposed protection method, a comparative performance assessment is presented in Table 1. The comparison benchmarks the CSI-based centralized scheme against the most widely used protection techniques in modern DC microgrids, including overcurrent-based protection and differential protection. The comparison emphasizes criteria that are fundamental for DC microgrids, including operational speed, selectivity, sensitivity to high-impedance faults, sensor requirements, and scalability. The table below summarizes the key distinctions.

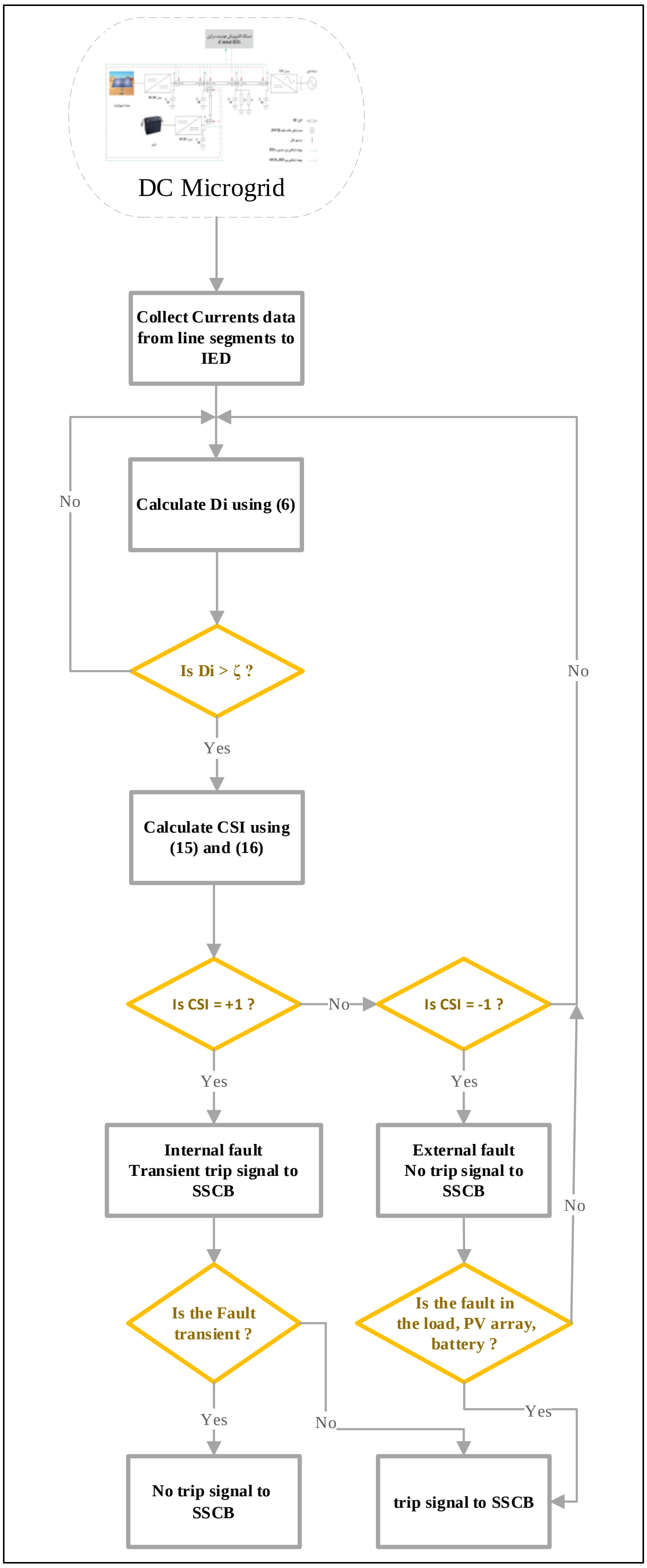

Figure 6. Diagram of the proposed protection algorithm.

As summarized in Table 1, the proposed CSI-based method demonstrates significant advantages over traditional approaches. Unlike overcurrent protection, which struggles to detect high-impedance faults and is highly sensitive to load fluctuations, the CSI algorithm remains stable under 85-115% load variations and accurately identifies internal faults even when fault current magnitude is very small. Differential protection provides higher accuracy but requires multiple synchronized measurements and becomes unreliable when the current difference falls below the detection threshold. In contrast, the CSI method relies solely on waveform similarity and does not depend on fault magnitude, enabling fast (<2 ms), selective, and cost-effective protection for DC microgrids. This makes it especially suitable for centralized telecom power systems where communication, hardware cost, and scalability are critical concerns.

Recent studies indicate a growing body of work on DC-microgrid protection, particularly for converter-dominated and low-voltage systems. Overcurrent relays remain the simplest solution but continue to struggle with high-impedance faults and load-induced transients in LVDC environments [25],[26].

Differential protection approaches improve selectivity but their performance can degrade when terminal current differences are small or when communication delays and synchronization errors arise in multi-terminal systems [23]. Directional and polarity-based techniques have also been studied; however, their reliability may be reduced during fast switching and voltage-distortion events caused by power-electronic converters [25],[27].

In parallel, transient-, signature-, and machine-learning–based schemes have been proposed to detect high-impedance and subtle faults by exploiting waveform features, wavelet coefficients, or classifier models; while effective, these approaches often require high sampling rates, synchronized measurements, or additional sensors that increase system complexity [28],[29]. Recently, cosine-similarity and other vector-similarity measures have been applied to transient waveform segments and traveling-wave heads for fault identification and localization, demonstrating strong discrimination capability and robustness to amplitude variations [30]-[32].

Taken together, these studies reveal a gap for a lightweight, communication-efficient, and load-transient-immune protection method tailored to 48-V telecom DC microgrids. The CSI-based method proposed here addresses that gap by comparing the directional similarity of di/dt waveforms at both line terminals. The approach does not rely on instantaneous fault magnitude, does not require voltage sensors or strict measurement synchronization, and remains resilient under normal load swings (≈85–115%), providing fast (<2 ms), selective, and cost-effective protection for telecom microgrids.

As summarized in Table 2, although the proposed CSI-based protection method was demonstrated using a 3.5 kW/48 V telecom test platform, the underlying mechanism is not tied to any specific DC voltage level or system rating. Because CSI evaluates the *shape similarity* of current waveforms rather than their absolute magnitude, its detection behavior remains consistent across different voltages, feeder lengths, and microgrid capacities. The centralized IED architecture also scales naturally to larger or more complex networks, with each additional feeder contributing only one current channel and the computational effort increasing linearly with system size. Consequently, the strengths highlighted in Table 2. Robust load-change immunity, low sensing requirements, and strong disturbance tolerance-remain valid for all classes of DC microgrids, including multi-node systems, distributed DC networks, and DC substation environments.

Table 1. Comparative performance of the proposed CSI-based method and contemporary protection approaches.

Directional / Other Unit Methods [6],[23],[24]	Differential Protection [19], [20]	Overcurrent Protection [6], [7]	Proposed CSI-Based Method	Criterion
3–10 ms	2–5 ms	10–50 ms	< 2 ms	Operating Speed
Medium	High	Low–Moderate	High (directional CSI comparison)	Selectivity Under Load Variations
Poor–Moderate	Fails when ΔI < threshold	Weak	Strong (magnitude-independent similarity)	High-Impedance Fault Sensitivity
2–3	4–6 sensors per line section	1 current sensor	2 current sensors per line	Sensor Requirement
Medium	High	None	Moderate (central IED)	Communication Dependence
Medium	Medium	Low	High (stable CSI under 85%–115% load swings)	Immunity to Load-Induced Transients
Moderate	Low–Medium	Medium	High	Scalability to Multi-Node Systems

Table 2. Comparative evaluation of the proposed CSI-based protection method and selected recent DC-microgrid.

Adaptive droop / derivative based [33]	Wavelet + singular value decomposition (SVD) for high resistance fault (HRF) [34]	Short-time Fourier transform (STFT) + Machine Learning (ML) [35]	Proposed CSI-Based Method	Metric
Weak–Moderate-derivative reacts to load steps	Moderate-HRF-oriented	Good-depends on ML training quality	Excellent	Load-change immunity
Weak - poor small-signal sensitivity	Very strong - explicit HRF detection	Not HIF-focused	Strong - CSI magnitude-independent	HIF / HRF detection capability
Very fast (few ms)	Tens of ms	Low-ms range	Fast - few ms (< 2 ms)	Detection time
Low–Moderate	High - wavelet + SVD processing	Moderate - high sampling for STFT	Low - only two current sensors	Sensor/measurement requirements
Low	Low–Medium	Low	Medium-centralized IED	Communication needs
Moderate	Moderate	Good	Excellent - voltage-independent	Applicability across DC microgrid voltage levels
Fast but limited	Very good for HRF	Good	Best balance of scalability + robustness + simplicity	Overall

5 Results

The proposed protection scheme was rigorously evaluated on the 48V DC microgrid architecture illustrated in Figure 3, with system specifications detailed in Table 3. Through comprehensive MATLAB/Simulink simulations, the following test scenarios were executed:

Table 3. DC microgrid components and parameters.

48 V DC	System Voltage
3.5 kW	Base power
48 V, 50 ah	Battery
4 kW	Battery DC-DC converter
$V_{mp} = 54.7$ V, $I_{mp} = 5.58$ A at STC	Solar panel
4 kW	PV converter
4 kW	VSC connecting to utility grid
base transceiver station load, 3.5 kW	Load
$0 - 2\ \Omega$	Fault resistance
25 mF	DC link capacitor

5.1 Fault detection and protection decision

The protection system was tested with a 0.8 Ω pole-to-ground fault applied to line bc for 100 ms, as illustrated in Figure 5. Current measurements and their derivatives from both ends of the line (Figure 7(a)-(d)) showed positive rates of change (di/dt) with synchronized increasing trends. The CSI calculated from these measurements yielded a value of +1 (Figure 7(e)), confirming an internal fault condition as specified by Equation (14). Upon fault identification, the IED issued tripping commands to the circuit breakers at both terminals of line bc.

The protection system responded within 2ms, successfully isolating the faulted section. The consistent directional relationship between current derivatives at the two-line ends-evident in their matching polarity and magnitude profiles in Figure 7 validates the algorithm's ability to distinguish internal faults from external disturbances. This result demonstrates the scheme's reliability in detecting internal faults while maintaining the rapid response required for DC microgrid protection.

Similarly, we investigate an external fault F_2 (Figure 5). This pole-to-ground fault is simulated with a resistance of 0.8 Ω and a duration of 100 ms in the ab line. The values of the measured currents and their change rates from both sides of the bc line are shown in Figure 8(a)-(d), respectively. Given that the current change averages on both sides of the line are in the opposite direction, Using Equation (14), the calculated CSI value is -1, indicating the occurrence of an external fault (As shown in Figure 8(e)). Thus, the IED sends a functional command to the circuit breaker of the line bc circuit.

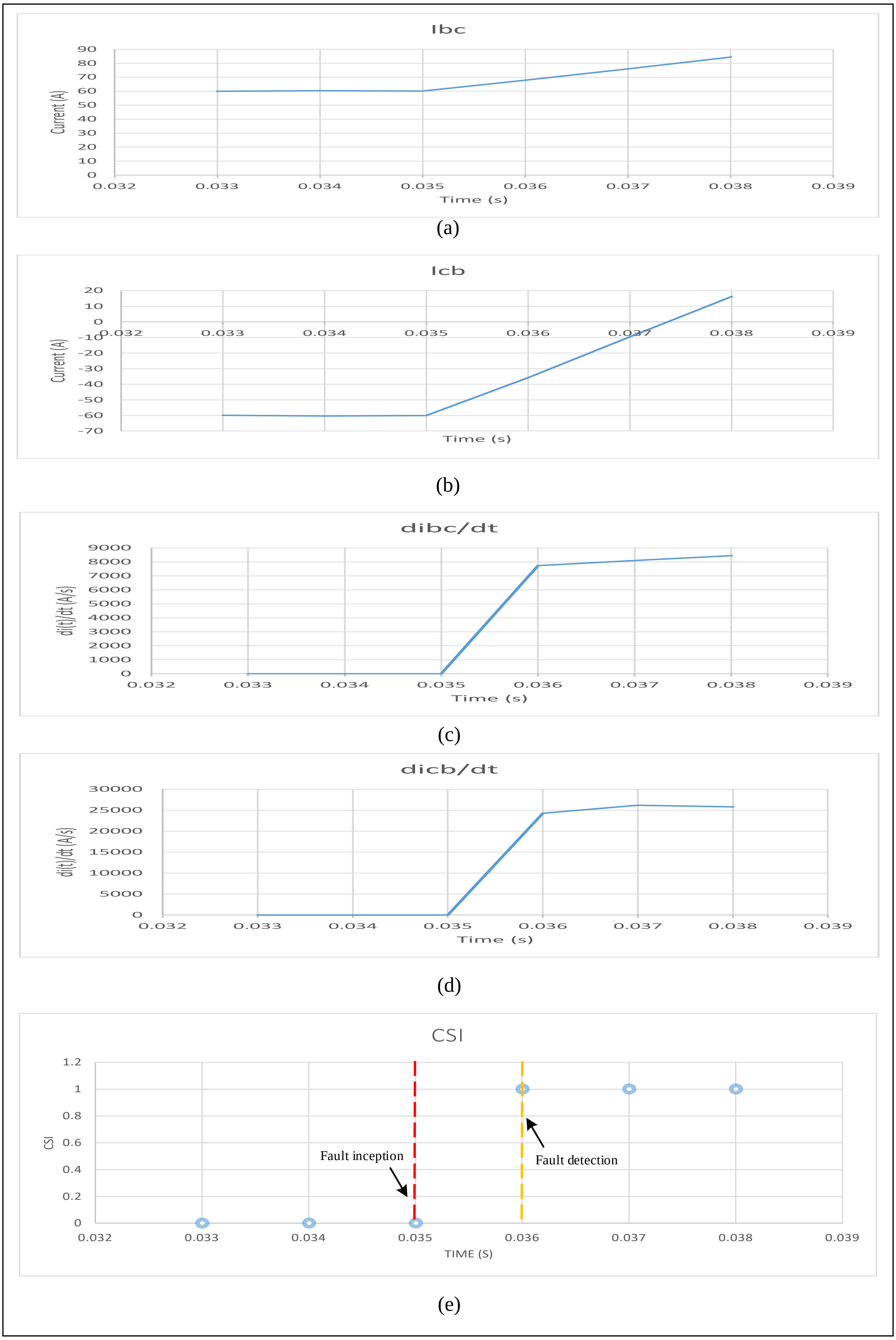

Figure 7. Internal fault F_1 in the bc line. (a); (b): Values of currents on sides b and c. (c); (d): Change rate of currents. (e): CSI obtained.

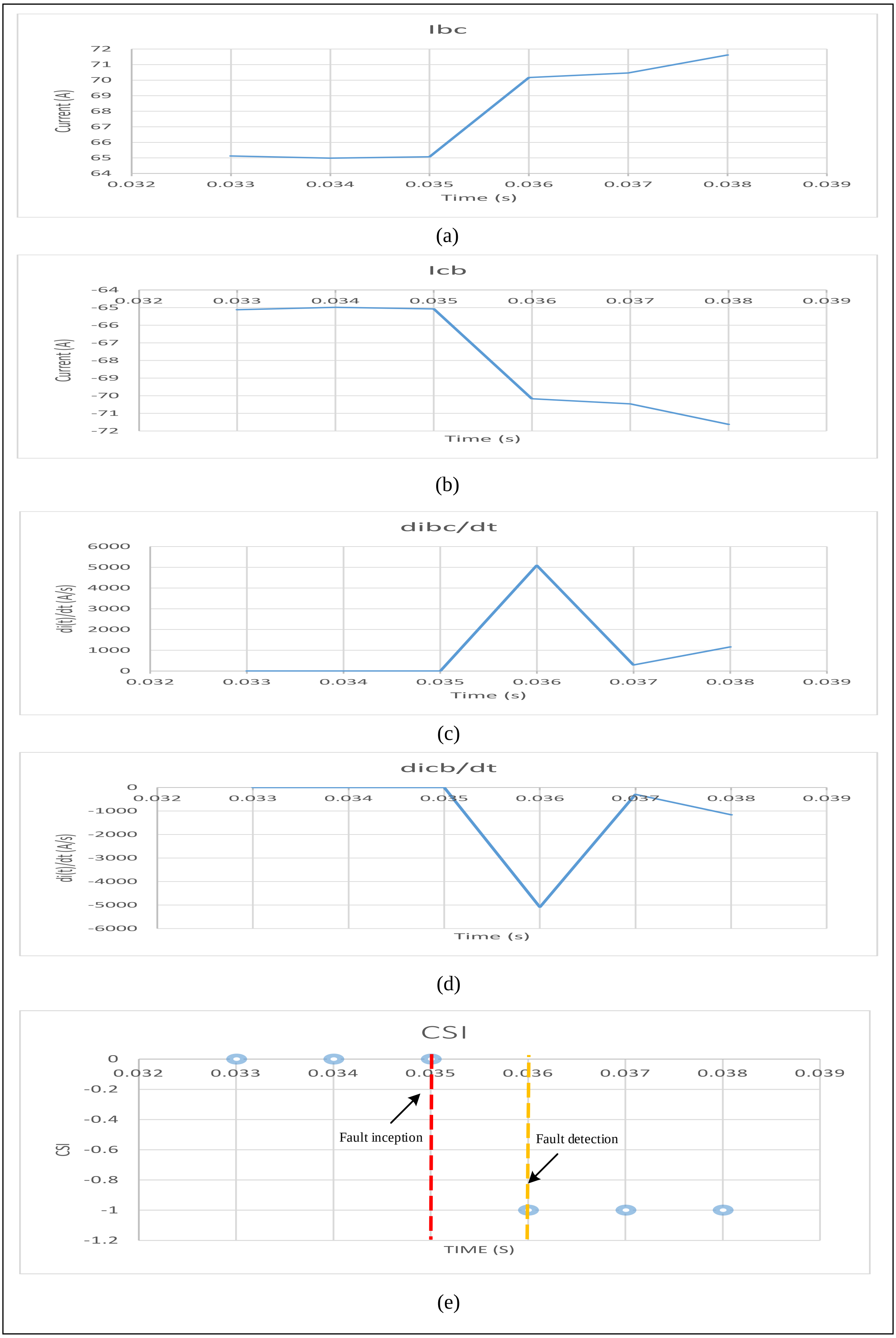

Figure 8. External fault F_2 in the ab line. (a); (b): Values of currents on sides b and c. (c); (d): Change rate of currents. (e): CSI obtained.

The performance of the presented method for sudden changes is also investigated. The algorithm maintained stability during extreme load fluctuations (86.3%-115.9% of nominal 3G telecommunication post load), consistently generating $CSI = -1$ outputs (Figure 9). This confirms reliable discrimination between actual faults and normal load transients.

In the following, the functional protection for temporary faults will be discussed. F_1 (Figure 5) is a pole-to-ground fault with a resistance of 0.8 Ω and is simulated as a transient fault with a duration of 1ms in line bc. The values of the measured currents and their change rates from both sides of the line are shown in Figure 10(a)-(d), respectively. Given that the current change averages on both sides of the line are positive, using Equation (14), the calculated CSI value is +1, indicating the occurrence of an internal fault (As shown in Figure 10(e)). Thus, the IED sends a functional command to the circuit breakers of the bc line. Then, once 1ms passes, the command to reconnect is sent to the circuit breakers of the bc line, and after re-checking the received parameters of the network, and if the fault persists, a functional command is sent to the circuit breakers of the bc line. Otherwise, this functional command is not sent to circuit breakers.

5.2 Fault detection in loads, pv array, battery and protection decision

To investigate the protection performance of a low impedance fault F_3, we investigate Figure 5. This pole-to-ground fault is simulated for 0.1 seconds in busbar c, where the loads are located. The calculated CSI in the lines yields a value of -1, as shown in Figure 11(a). According to the investigation, the currents passing through the cb and ce sensors exceed the threshold of the currents, indicating the presence of a fault. Then, the IED sends the functional command to circuit breakers cb and ce, as shown in Figure 11(b), (c).

5.3 Performance during equipment failure and communication link failure

The proposed protection scheme maintains reliable operation even during partial system failures. When one or two-line sensors or their communication links fail, the method preserves both decision accuracy and proper selectivity. This resilience is achieved through the central IED's comprehensive data integration capability, which reconstructs missing sensor data by applying Kirchhoff's Current Law (KCL) to measurements from adjacent line sensors.

Furthermore, the system demonstrates fault tolerance for breaker operation failures. If a line circuit breaker or its communication link fails to respond to IED commands - despite receiving both the activation signal and valid current measurements from line sensors-the IED automatically redirects the tripping command to adjacent line breakers. This redundant protection mechanism ensures continuous fault isolation capability even during equipment malfunctions.

In line with IEC 61850 concepts of dependability and security in protection systems, the centralized IED also handles communication issues gracefully. The CSI-based algorithm does not rely on strict real-time synchronization between feeders, so short delays or temporary drops in data do not affect decision-making. If a communication link or sensor channel becomes unavailable, the IED simply marks that channel as out of service while continuing normal protection for all remaining feeders. This localized handling ensures that a single failure-whether a sensor, breaker, or communication link-does not compromise system-wide protection. Overall, the behavior of the scheme aligns with the IEC 61850 philosophy: faults are contained, protection remains available, and the system continues operating securely even when individual components fail.

6 Conclusion

This study presents a novel protection scheme for centralized DC microgrids in BTS applications. The proposed method detects internal faults by analyzing the similarity in current rate-of-change measurements from both terminals of each line segment. Comprehensive evaluation demonstrates the scheme's effectiveness in: (1) high-impedance fault detection, (2) permanent versus transient fault discrimination, and (3) reliable protection of critical components including loads, PV arrays, and battery systems. The design maintains functionality even during sensor or circuit breaker failures, demonstrating robust fault tolerance.

Unlike conventional approaches requiring extensive voltage and current monitoring infrastructure, our solution offers a cost-effective alternative utilizing just one centralized IED per microgrid with only two current sensors per line segment (one at each terminal). MATLAB/Simulink simulations validate the scheme's performance for both internal and external fault scenarios, confirming its operational reliability under various grid conditions.

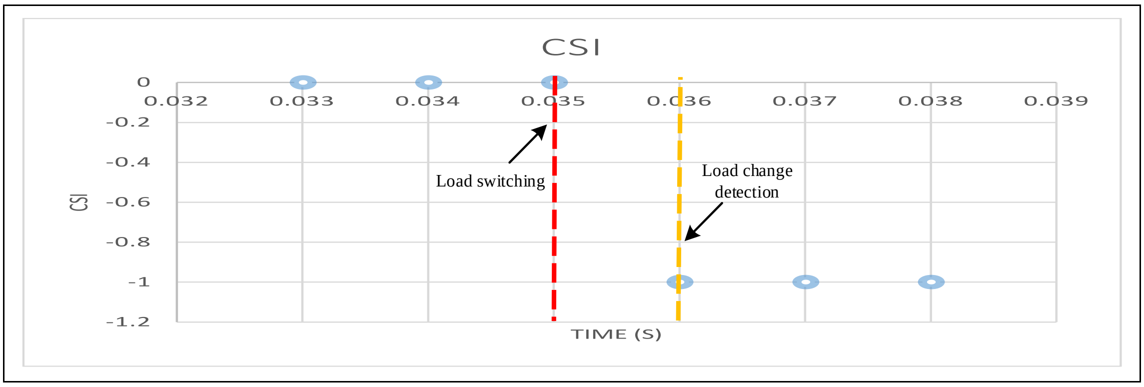

Figure 9. CSI obtained for sudden load change.

Figure 10. Internal transient fault F_1 in the bc line: (a),(b) Values of currents on sides b and c, (c),(d) Change rate of currents, (e) CSI obtained.

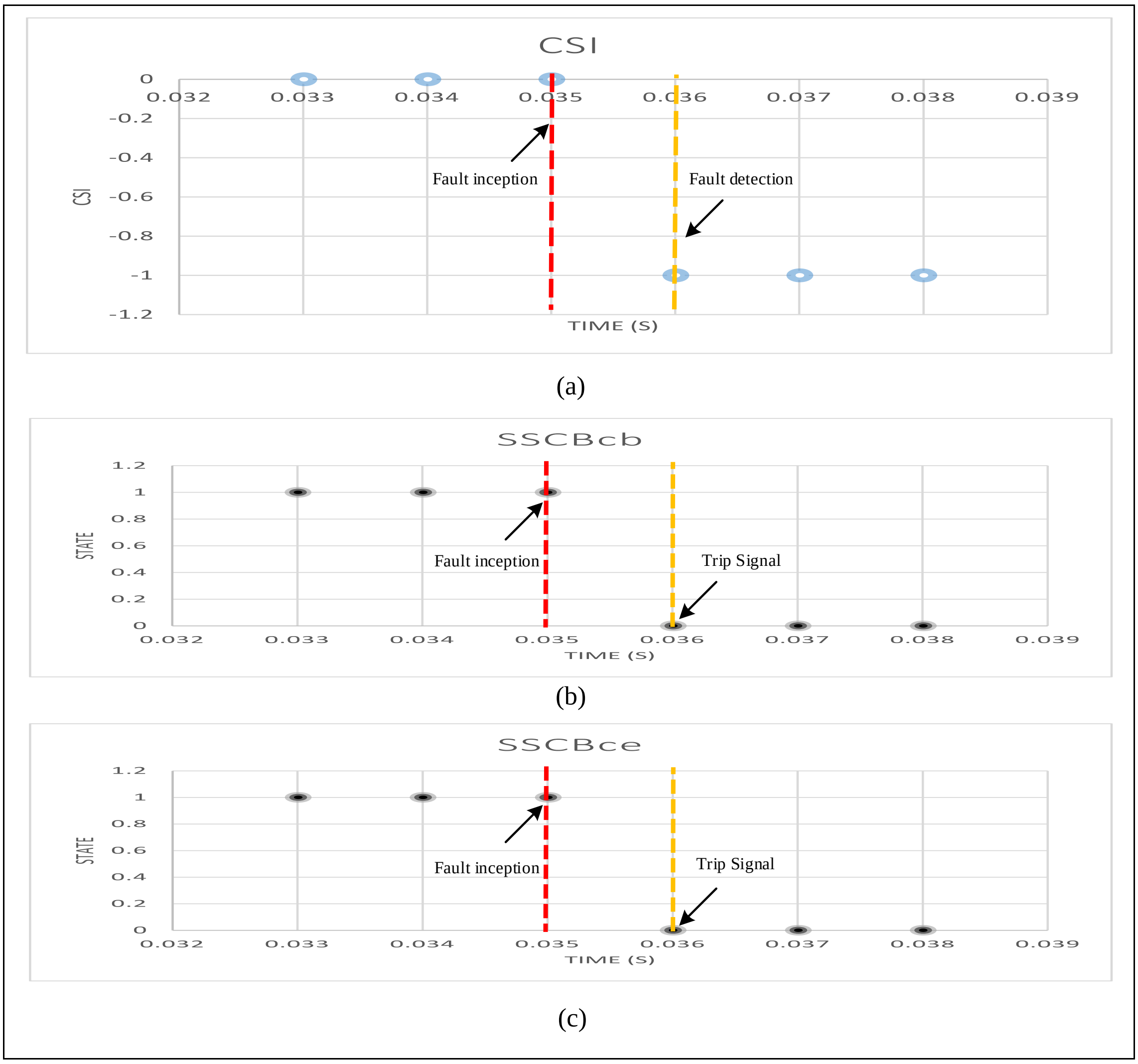

Figure 11. F_3 low impedance fault at bus C. (a): CSI obtained from the lines. (b); (c): Function modes of $SSCB_{cb}$ and $SSCB_{ce}$ at the time of the fault.

7 Author contribution statements

Mohammad Reza Kochehbiuki, contributed to the conception of the study, design and modeling of the DC microgrid system, performing the simulations and analyses, interpretation of the results, as well as writing and revising the manuscript. Alireza Sedighi Anaraki, contributed to the writing, language editing, critical revision of the manuscript, and provided general supervision during the study. Mohammad Reza Mazidi, acted as an advisor and provided guidance and valuable suggestions in several stages of the research.

8 Ethics committee approval and conflict of interest statement

"There is no need to obtain permission from the ethics committee for the article prepared". "There is no conflict of interest with any person / institution in the article prepared".

9 Reference

[1] Justo JJ, Mwasilu F, Lee J, Jung JW. "AC-microgrids versus DC-microgrids with distributed energy resources: A review". *Renewable and Sustainable Energy Reviews*, 24, 387-405, 2013.

[2] Ojo JS, Owolawi PA, Atoye AM. "Designing a green power delivery system for base transceiver stations in Southwestern Nigeria". *SAIEE Africa Research Journal*, 110(1), 19-25, 2019.

[3] Rami G, Tran-Quoc T, Hadjsaid N, Mertz J. "Energy supply for remote base transceiver stations of telecommunication". *IEEE Power Engineering Society General Meeting*, Denver, CO, USA, 6-10 June 2004.

[4] Chandra A, Singh GK, Pant V. "Protection techniques for DC microgrid-A review". *Electric Power Systems Research*, 187, 106439, 2020.

[5] Mirsaeidi S, Dong X, Said DM. "Towards hybrid AC/DC microgrids: Critical analysis and classification of protection strategies". *Renewable and Sustainable Energy Reviews*, 90, 97-103, 2018.

[6] Zhang L, Tai N, Huang W, Liu J, Wang Y. "A review on protection of DC microgrids". *Journal of Modern Power Systems and Clean Energy*, 6(6), 1113-1127, 2018.
[7] Baidya S, Nandi C. "A comprehensive review on DC Microgrid protection schemes". *Electric Power Systems Research*, 210, 108051, 2022.
[8] Modu B, Abdullah MP, Sanusi MA, Hamza MF. "DC-based microgrid: Topologies, control schemes, and implementations". *Alexandria Engineering Journal*, 70, 61–92, 2023.
[9] Beheshtaein S, Cuzner R, Savaghebi M, Guerrero JM. "Review on microgrids protection". *IET Generation, Transmission & Distribution*, 13(6), 743–759, 2019.
[10] Mohanty R, Sahoo S, Pradhan AK, Blaabjerg F. "A cosine similarity-based centralized protection scheme for dc microgrids". *IEEE Journal of Emerging and Selected Topics in Power Electronics*, 9(5), 5646–5656, 2021.
[11] Fletcher SDA, Norman PJ, Galloway SJ, Crolla P, Burt GM. "Optimizing the roles of unit and non-unit protection methods within DC microgrids". *IEEE Transactions on Smart Grid*, 3(4), 2079-2087, 2012.
[12] Meghwani A, Srivastava SC, Chakrabarti S. "A non-unit protection scheme for DC microgrid based on local measurements". *IEEE Transactions on Power Delivery*, 32(1), 172–181, 2016.
[13] Saleh KA, Hooshyar A, El-Saadany EF. "Hybrid passive-overcurrent relay for detection of faults in low-voltage DC grids". *IEEE Transactions on Smart Grid*, 8(3), 1129-1138, 2015.
[14] Fletcher SD, Norman PJ, Fong K, Galloway SJ, Burt GM. "High-speed differential protection for smart DC distribution systems". *IEEE Transactions on Smart Grid*, 5(5), 2610–2617, 2014.
[15] Park J-D, Candelaria J. "Fault detection and isolation in low-voltage DC-bus microgrid system". *IEEE Transactions on Power Delivery*, 28(2), 779-787, 2013.
[16] Yuan C, Haj-Ahmed MA, Illindala MS. "Protection strategies for medium-voltage direct-current microgrid at a remote area mine site". *IEEE Transactions on Industry Applications*, 51(4), 2846–2853, 2015.
[17] Emhemed AAS, Burt GM. "An advanced protection scheme for enabling an LVDC last mile distribution network". *IEEE Transactions on Smart Grid*, 5(5), 2602–2609, 2014.
[18] Lai Q, Zhang Z, Zhang K, Yin X, Chen Y. "Research on Pilot Protection for Tie Line of Renewable Energy Sources". *IEEE Access*, 11, 1613–1628, 2023.
[19] Zheng L, Jia K, Wu W, Liu Q, Bi T, Yang Q. "Cosine similarity based line protection for large scale wind farms part II-the industrial application". *IEEE Transactions on Industrial Electronics*, 69(3), 2599–2609, 2021.
[20] Sirisha A, Pradhan AK. "Cosine similarity based directional comparison scheme for subcycle transmission line protection". *IEEE Transactions on Power Delivery*, 35(5), 2159-2167, 2019.
[21] Jia K, Wang C, Bi T, Zhu R, Xuan Z. "Transient current waveform similarity based protection for flexible DC distribution system". *IEEE Transactions on Industrial Electronics*, 66(12), 9301–9311, 2019.
[22] Augustine S, Brahma S, Quiroz JE, Reno MJ, . "DC Microgrid Protection: Review and Challenges". Sandia National Laboratories, Albuquerque, New Mexico, USA, Sandıa Report SAND2018-8853, 2018.
[23] Binqadhi H, Hamanah WM, Shafiullah M, Alam MS, AlMuhaini MM, Abido MA. "A comprehensive survey on advancement and challenges of DC microgrid protection". *Sustainability*, 16(14), 6008, 2024.
[24] Haleem NM, Rajapakse AD. "Application of new directional logic to improve DC side fault discrimination for high resistance faults in HVDC grids". *Journal of Modern Power Systems and Clean Energy*, 5(4), 560–573, 2017.
[25] Alam MS, Al-Ismail FS, Rahman SM, Shafiullah M, Hossain MA. "Planning and protection of DC microgrid: A critical review on recent developments". *Engineering Science and Technology, an International Journal*, 41, 101404, 2023.
[26] Bayati N, Hajizadeh A, Soltani M. "Protection in DC microgrids: a comparative review". *IET Smart Grid*, 1(3), 66-75, 2018
[27] Bayati N, Balouji E, Baghaee HR, Hajizadeh A, Soltani M, Lin Z, Savaghebi M. "Locating high-impedance faults in DC microgrid clusters using support vector machines". *Applied Energy*, 308, 118338, 2022.
[28] Bera PK, Kumar V, Pani SR, Bargate V. "Detection of high impedance faults in microgrids using machine learning". *IEEE 2022 Green Energy and Smart Systems Conference (IGESSC),* Long Beach, CA, USA, 7-8 November 2022*.*
[29] Grcić I, Pandžić H. "High-Impedance Fault Detection in DC Microgrid Lines Using Open-Set Recognition". *Applied Sciences*, 15(1), 193, 2024.
[30] Jarrahi MA, Samet H, Ghanbari T. "Protection framework for microgrids with inverter-based DGs: A superimposed component and waveform similarity-based fault detection and classification scheme". *IET Generation, Transmission & Distribution*, 16(11), 2242–2264, 2022.
[31] Zhao J, Zhang Y, Yuan Y, Li Y. "Microgrid line protection method using the cosine similarity of the time domain traveling waveform". *International Journal of Electrical Power & Energy Systems*, 153, 109335, 2023.
[32] Zhao R, Lu J, Yu Z, Yu Z, Wu Y, Wang K. "A two-stage fault localization method for active distribution networks based on COA-SVM model and cosine similarity". *Electronics*, 13(19), 3809, 2024.
[33] Augustine S, Reno MJ, Brahma SM, Lavrova O. "Fault current control and protection in a standalone DC microgrid using adaptive droop and current derivative". *IEEE Journal of Emerging and Selected Topics in Power Electronics*, 9(3), 2529–2539, 2020.
[34] Jing L, Zhao T, Xia L, Zhou J. "An improved high-resistance fault detection method in DC microgrid based on orthogonal wavelet decomposition". *Applied Sciences*, 13(1), 393, 2022.
[35] Grcić I, Pandžić H, Novosel D. "Fault detection in DC microgrids using short-time fourier transform". *Energies*, 14(2), 277, 2021.